RSC Advances

ROYAL SOCIETY OF CHEMISTRY

www.rsc.org/advances

RSC Advances

ARTICLE

Dye-sensitized solar cells based on a 1D/3D double-layered ZnO photoanode with improved photovoltaic performance

Yu-Fen Wang[a,b], Xin Wang[a], Xi-Fei Li*[a] and De-Jun Li*[a]

Received 00th January 20xx,
Accepted 00th January 20xx

DOI: 10.1039/x0xx00000x

www.rsc.org/

The engineered metal oxide anode materials highly affect photovoltaic performance of solar cells. In this research, we fabricate double-layered ZnO nanoarrys (NRs)/ellipsoids or spheres films on fluorine-doped tin oxide (FTO) substrate as photoanodes for dye-sensitized solar cells (DSSCs). The results indicate that DSSCs based on the double-layered ZnO NRs/spheres film (~3.19 %) show an obvious 41.2 % enhancement of power conversion efficiency (PCE) as compared to the ZnO NRs/ellipsoids film (~2.26 %), which are confirmed by the IMPS, IMVS, EIS and UV-vis diffused reflectance study. This study provides a scheme to selective combination of specific ZnO morphologies into an ideal photoanode configuration with more dye loading and superior light scattering ability for enhanced photovoltaic performance.

1. Introduction

In modern-day society, the excessive exhaustion of fossil fuels and rising global energy demand have driven the development of new types of renewable and sustainable alternatives. Due to relatively high solar-to-light conversion efficiency, low-cost and environment benign fabrication process, Dye-sensitized solar cells (DSSCs) have been regarded as one of the most promising candidates for the future class of affordable photovoltaic devices.[1,2] So far, more than 13 % PCE has been reported through the continuous efforts on optimization of photoanodes, sensitizers, electrolytes and counter electrodes.[3] Apart from the widely investigated TiO_2 photoanode, other metal oxide semiconductors, such as ZnO,[4, 5] SnO_2[6-8] and Zn_2SnO_4,[9-12] also have received a great deal of attention. ZnO, as an alternative metal oxide anode material in DSSCs, exhibits several advantages such as higher electron mobility (205-300 $cm^2\ V^{-1}\ S^{-1}$),[13] wide band gap (3.37 eV) as well as a large excitation binding energy (60 meV) at room temperature.[14]

The ZnO NRs photoanodes have been widely investigated due to their faster electron transport rate, slower recombination rate and excellent light scattering ability. However the smaller surface area ascribed to the large diameter and free space between the neighboring 1D structure results in less amount of the dye anchoring and thus limits the photovoltaic performance of the DSSCs. ZnO nanowire arrays photoanodes for high efficiency DSSCs (η=1.5–2.4 %) were reported.[15, 16] The PCE of the DSSC with well aligned ZnO nanorod/ITO electrode is 3.15% reported by Jung *et. al*.[17] One of the solutions to address this drawback is to construct hierarchically structured anode materials, which possess a higher specific surface area to absorb sufficient amounts of dye molecules, a well-organized structure for faster electron transport rate, and a microfeature size for superior light scattering capability.[18-21] These types of anode materials have been proved to further improve the DSSCs performance in an efficient mannar.

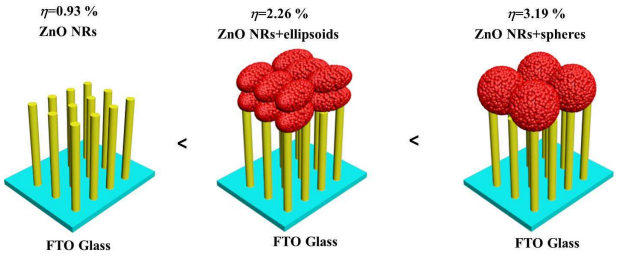

Scheme 1 Schematic illustration of the three kinds of photoanodes (**ZnO NRs**, **ZnO NRs+ellipsoids**, **ZnO NRs+spheres**).

In the present work, the integration of 1D structures and 3D hierarchical ellipsoids or spheres into a 1D/3D double layered photoanode consisting of ZnO nanorods (bottom layer) and ZnO ellipsoids or spheres (top layer). Scheme 1 is the schematic illustration of the three kinds of photoanode structures (**ZnO NRs**, **ZnO NRs+ellipsoids**, **ZnO NRs+spheres**) for the present DSSCs study. This design combines the advantages of ZnO nanorods (faster electron transport rate, slower electron recombination rate) and ZnO ellipsoids or spheres (more amount of dye adsorption, excellent light scattering ability). Fig. S1 shows the cross-sectional FE-SEM image of ZnO NRs+ellipsoids and ZnO NRs+spheres double layered photoanode film. There is no obvious gap between ZnO ellipsoids or spheres top layer and nanorods active layer, indicating the connectivity between ZnO ellipsoids or spheres and nanorods is quite good, which is suitable for the efficient charge transport from ZnO ellipsoids or spheres to nanorods.

[a] *Energy & Materials Engineering Centre, College of Physics and Materials Science, Tianjin Normal University, Tianjin 300387, China. E-mail: xfli@mail.tjnu.edu.cn; dejunli@mail.tjnu.edu.cn; Tel: +86-22-23766526, Fax: +86-22-23766503*
[b] *Key Laboratory of Advanced Energy Materials Chemistry (Ministry of Education), Collaborative Innovation Center of Chemical Science and Engineering, College of Chemistry, Nankai University, Tianjin 300071, China.*
Electronic Supplementary Information (ESI) available: [XRD and FE-SEM of ZnO nanorods]. See DOI: 10.1039/x0xx00000x

Here, a simple sonochemical process without the surfactant to synthesize 3D hierarchical ZnO ellipsoids or spheres has been developed. As a result, the DSSC based on ZnO NRs+ ellipsoids or spheres double-layered photoanode shows an efficiency of 2.26 % and 3.19 %, respectively, which are much higher than that of the ZnO NRs counterpart (0.93 %). And the DSSC based on ZnO NRs+ spheres double-layered photoanode shows a higher efficiency (3.19 %) than that of well aligned ZnO nanorod/ITO electrode (3.15 %).[17]

2.Results and discussions

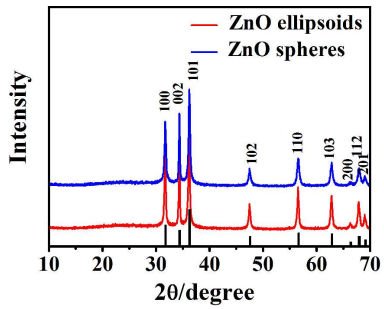

Fig. 1 (a) XRD patterns of as-synthesized ZnO ellipsoids or spheres samples after sonochemical reaction for 10 min.

The crystal phase of the as-prepared ZnO samples prepared by sonochemical reaction are examined by powder X-ray diffraction (XRD), as shown in Fig. 1. The diffraction peaks of the as-prepared sample are consistent with the hexagonal structure of ZnO (JCPDS Card No. 65-3411) with cell constants of a=b=3.25 Å and *c* = 5.207 Å, and the strong peaks of the XRD patterns indicates high crystallinity of the as-prepared ZnO.

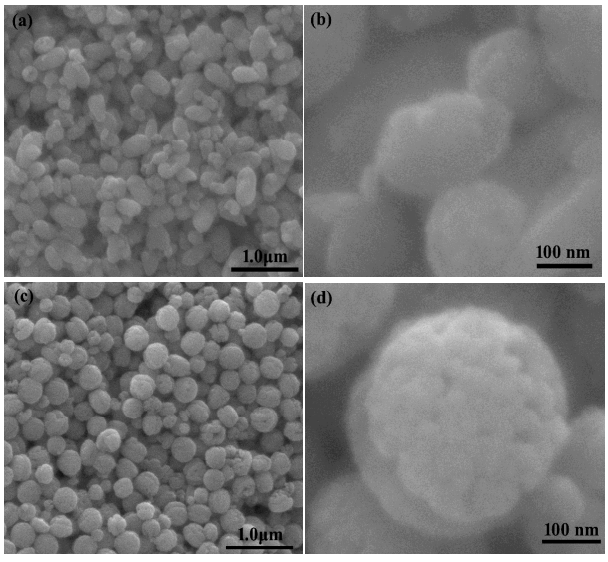

Fig. 2. FE-SEM images of as-prepared (a-b) ZnO ellipsoids and (c-d) ZnO spheres, respectively.

The morphologies of the as-prepared ZnO samples are characterized by field emission scanning electron microscopic (FE-SEM), shown in Fig. 2. Interestingly, the ZnO ellipsoids (~150 nm in diameter, ~250 nm in length) are clearly observed via the present simple and fast sonochemical reaction (10 min), as shown in Fig. 2a, b. It can be seen that the as-synthesized ZnO products exhibit hierarchical spherical structure of ~350 nm in diameter (Fig. 2c, d) in the presence of diethylene glycol (DEG). These results indicate that DEG is of importance for the formation of ZnO spheres, which is probably affected by the kinetic control. It is well known that the growth rate is different along the different crystallographic directions, and the faster growth plane determines the final morphology.[22] The influences of DEG on the ZnO morphology may be attributed to its coordination property with Zn^{2+} and the reactivity, which will change the nuclei and growth rates of different crystal directions and lead to different morphologies and sizes of the products. In addition, the way that DEG exactly works still needs to be further studied. From the higher magnification FE-SEM image (Fig. 2b, d) one can clearly found that the hierarchical ZnO ellipsoids or spheres are consisting of small well-interconnected nanoparticles.

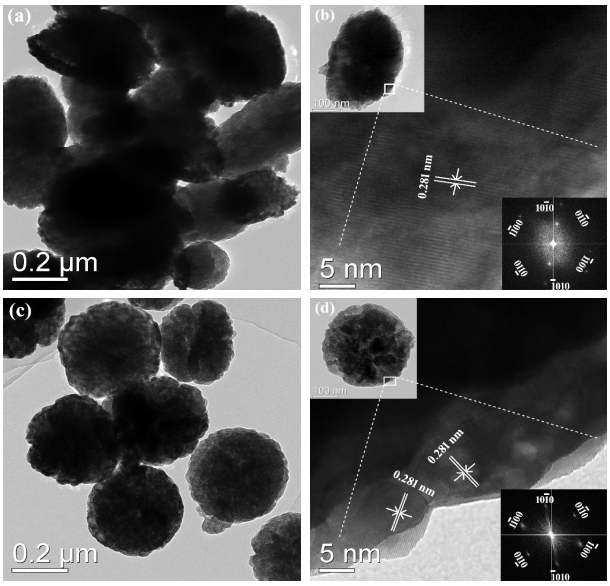

Fig. 3 (a) TEM image of as-prepared ZnO ellipsoids. (b) The HRTEM image of an individual ZnO ellipsoid, insets in upper and lower are the corresponding TEM image and FFT image of ellipsoid. (c) TEM image of as-prepared ZnO spheres. (d) The HRTEM image of an individual ZnO sphere, insets in upper and lower are the corresponding TEM image and FFT image of sphere.

The as-synthesized ZnO products are further characterized by transmission electron microscopy (TEM), as shown in Fig. 3. The low-magnification TEM image (Fig. 3a) clearly reveals the ZnO ellipsoids morphology which is ~150 nm in diameter and ~250 nm in length (individual ZnO ellipsoid, inset in Fig. 3b, left upper). Their morphological characters are in good agreements with the corresponding FE-SEM results in Fig. 2 a, b. The HRTEM image (Fig. 3b) shows that the ZnO nanopartices (building blocks of ellipsoid) exhibit obvious lattice fringes with the lattice space of 0.281 nm,

which can be indexed as (10$\bar{1}$0) planes of ZnO. Furthermore, the corresponding Fast Fourier Transform (FFT) image (inset in Fig. 3b, right lower) also confirms the single crystal nature of ZnO nanoparticles. Fig. 3c displays the typical TEM image of as-prepared hierarchical ZnO spheres, and the diameter is ~350 nm (inset in Fig. 3d, left upper). The HRTEM image in Fig. 3d clearly displays the resolved lattice fringes of 0.281 nm, which corresponds to the (10$\bar{1}$0) planes of ZnO. The FFT (inset in Fig. 3d, right lower) also demonstrates the single crystal nature of the ZnO nanoparticles, which is in agreement with the HRTEM observations.

The ZnO ellipsoids and spheres are screen-printed onto the surface of FTO/ZnO nanoarrys (NRs) electrode (Supporting Information, Fig. S2) to form 1D/3D double-layered photoanodes for DSSCs. The performance of N719-sensitized DSSCs based on different photoanodes was investigated by measuring the current density-voltage (*J-V*) curves under one sun illumination (100 mW cm^{-2}), as shown in Fig. 4a. The details of photovoltaic parameters, such as short-circuit current density (J_{sc}), open-circuit voltage (V_{oc}), fill factor (FF) and power conversion efficiency (PCE) are listed in Table 1. Obviously, the ~10.0 μm **ZnO NRs** based DSSCs show the lowest J_{sc} (3.35 mA cm^{-2}) and PCE (0.93 %) due to the insufficient amount of dye loading. With the 1D/3D double-layered photoanode, the J_{sc} of **Cell ZnO NRs+ellipsoids and Cell ZnO NRs+spheres** obviously increases up to 7.41 mA cm^{-2} and 10.66 mA cm^{-2}, respectively, due to the enhancement in adsorbed dye amounts. However, the V_{oc} (588 mV for **Cell ZnO NRs+ellipsoids**, 555 mV for **Cell ZnO NRs+ spheres**) decreases due to the augmentation of the surface area, which would provide additional charge-recombination sites. Furthermore, the FF of the 1D/3D double photoanodes shows no obvious changes. As a result, the PCE of DSSCs based on **ZnO NRs+ellipsoids** is 2.26 %, while a higher PCE of 3.19 % has been witnessed for **Cell ZnO NRs+ spheres**. The enhancement of the photovoltaic performance for the **Cell ZnO NRs+ spheres** is mainly ascribed to the improvement of J_{sc} and PCE.

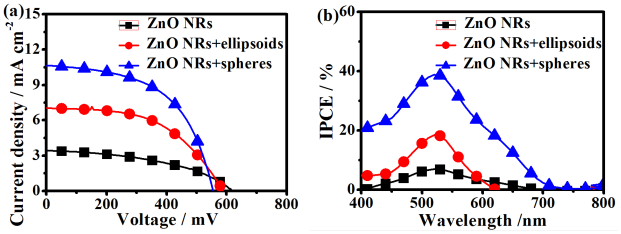

Fig. 4 (a) Photocurrent density-voltage (*J-V*) and (b) IPCE curves for DSSCs based on different Cells (**ZnO NRs**, **ZnO NRs+ellipsoids**, **ZnO NRs+spheres**).

The incident-photon-to-current conversion efficiency (IPCE) spectra are performed to further understand the scattering effect, as is shown in Fig. 4b. It clearly illustrates that the IPCE value of **Cell ZnO NRs+spheres** is higher than that of **Cell ZnO NRs+ellipsoids** in all wavelength region from 400 nm to 800 nm. For instance, the obtained IPCE value of the former is 40.0 % at 525 nm (corresponding to the N719 absorption peak), which is higher than that of **Cell ZnO NRs+ellipsoids (**18.5 %**)**.[23]

Table 1. Detailed photovoltaic parameters (J_{sc}, V_{oc}, FF, and PCE) of DSSCs with different ZnO photoanodes.

DSSCs	J_{sc} / mA cm^{-2}	V_{oc} / mV	η/%	FF	Adsorbed dye/ $\times10^{-8}$ mol cm^{-2}
ZnO NRs	3.35	618	0.93	0.45	1.27
ZnO NRs+ellipsoids	7.41	588	2.26	0.52	2.26
ZnO NRs+spheres	10.66	555	3.19	0.54	3.20

It is well known that the adsorbed dye amounts on photoanodes significantly affect the photocurrent as well as the overall PCE. The different N719 sensitized ZnO photoanodes are soaked into 0.1 M NaOH (3 mL), and the UV-vis absorption spectra of the desorbed N719 dye are used to calculate the amount of dye adsorbed on the ZnO photoanodes. It is found that the dye amount adsorbed on the **Cell ZnO NRs+spheres** (3.20×10^{-8} mol cm^{-2}) is higher than that of the **Cell ZnO NRs+ellipsoids** (2.26×10^{-8} mol cm^{-2}) and the **Cell ZnO NRs** (1.27×10^{-8} mol cm^{-2}). The results are in good agreement with the observed highest J_{sc} and PCE of **Cell ZnO NRs+spheres** shown in Table 1.

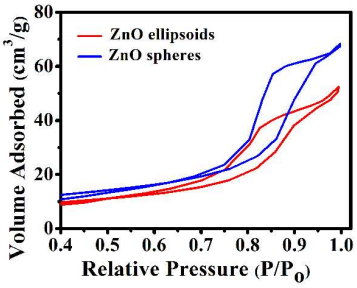

Fig. 5 N_2 adsorption-desorption isotherm curves of the ZnO ellipsoids and spheres samples.

The specific Brunauer-Emmett-Teller (BET) surface area of hierarchically ZnO spheres obtained from the N_2 adsorption-desorption measurements are shown in Fig. 5, a characteristic hysteresis loop can be observed in the plot at higher relative pressures, indicating the presence of mesopores in hierarchical ellipsoids and spheres generated from adjacent nanoparticles building blocks. The surface areas are 46.91 $m^2\ g^{-1}$ and 58.36 $m^2\ g^{-1}$ for ZnO ellipsoids and spheres, respectively. The different surface area of the ZnO ellipsoids and spheres leads to the different dye amounts, hence, the amount of adsorbed dye on ellipsoid loaded ZnO film should lower than that on spheres loaded film, and the results are also agreed with the observed amount of adsorbed dye in Table 1.

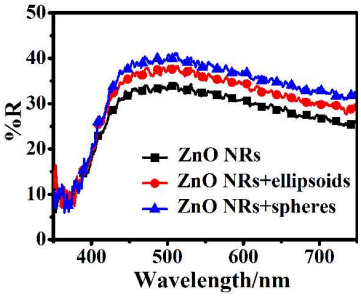

Fig. 6 Diffused reflectance spectra of three films without N719 dye (**Film ZnO NRs**; **Film ZnO NRs+ellipsoids**; **Film ZnO NRs+spheres**).

Besides the dye loading capacity, the light scattering effect can influence the light transport pathway within the ZnO photoanode film, which would affect the light-harvesting efficiency and thus the photovoltaic performance. The UV-vis diffused reflectance spectra of three ZnO films without N719 dye adsorption are measured to investigate the light-scattering ability of different photoanodes, as shown in Fig. 6. In the wavelength range of 400-750 nm, the ~10.0 μm **ZnO NRs Film** shows the lowest reflectance ability than those of double-layered ZnO film (~15.0 μm) due to the thinner film thickness. And the **Film ZnO NRs+spheres** (~ 10 μm ZnO NRs + ~ 5.0 μm ZnO spheres) shows much higher reflectance ability than **Film ZnO NRs+ellipsoids** (~ 10 μm ZnO NRs + ~ 5.0 μm ZnO ellipsoids). This clearly highlights the superior light scattering capability of the 1D/3D double layered **ZnO NRs+spheres** film. The hierarchical ZnO spheres top layer could effectively scatters the incident light and also multiple the optical pathway within the 1D/3D double layered films, resulting in significant improvement of the light absorption, and hence greatly contribute to the significant enhancement of the J_{sc}. Fig. S3 shows the *J–V* curve of the **Cell ZnO NRs+ellipsoids** (~ 10 μm ZnO NRs + ~ 9.0 μm ZnO ellipsoids), it is notable that the J_{sc}, V_{oc} and PEC is 9.38 mA cm^{-2}, 516 mV and 2.47 %, respectively, which are much lower PEC than **Cell ZnO NRs+spheres** (~ 10 μm ZnO NRs + ~ 5.0 μm ZnO spheres) despite they with the same adsorbed N719 dye amounts (Supporting Information,Table S1).These results are also agreed with the observed J_{sc} in Table 1. Based all above discussion, Cell double-layered **ZnO NRs/spheres** has improved efficiency than Cell **ZnO NRs/ellipsoids** is mainly attributed to the ZnO morphology.

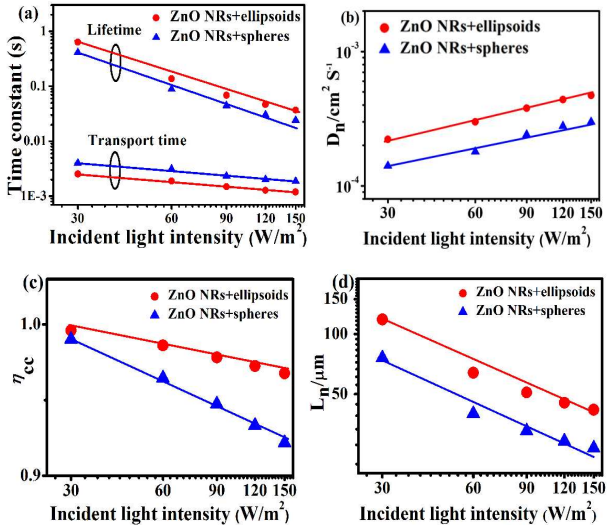

Fig. 7 (a) Light intensity dependent electron transport time and lifetime, (b) electron diffusion coefficient, (c) charge collection efficiency and (d) effective electron diffusion length of DSSCs based on different double-layered photoanodes (**ZnO NRs+ellipsoids**; **ZnO NRs+spheres**).

Intensity-modulated photocurrent spectroscopy (IMPS) and intensity-modulated photovoltage spectroscopy (IMVS) have been widely used as powerful tools to study the electron transport and charge recombination dynamics within the DSSCs photoanode films.[24] The IMPS and IMVS are conducted under illumination of a LED light source (λ= 457 nm) with different light intensities from 30 to 150 W/m^2, and the corresponding curves of the two 1D/3D double layered ZnO photoanodes based DSSCs are shown in Fig. 7a. The electron transport time ($\tau_d=1/2\pi f_d$; f_d is the characteristic frequency minimum of the IMPS imaginary component) and the electron lifetime ($\tau_r=1/2\pi f_r$; f_r is the characteristic frequency minimum of the IMVS imaginary component) as a function of light intensity is studied.[25, 26] The τ_d decrease with the increased light intensity because the deep traps are filled by the more photoelectrons generated at higher light intensity, resulting in electron trapping/detrapping involves shallower levels.[27] In Fig. 7a, the IMPS results clearly illustrate that the τ_d of the DSSC based on **Cell ZnO NRs+ellipsoids** photoanode is shorter than that of bare **Cell ZnO NRs+spheres** photonanode, implying that the former has faster electron transport rate due to the efficient transport path of ZnO ellipsoids. It is believed that the τ_r can reflect the recombination processes between the electron in conduction band of ZnO and I_3^- in the electrolyte. Thus, the τ_r decrease with the increase of light intensity may result from the larger recombination probability since more electrons exist in the conduction band of ZnO semiconductor. In Fig. 7a, the τ_r of **Cell ZnO NRs+ellipsoids** is longer than that of **Cell ZnO NRs+spheres**, indicating the longer electron lifetime and resulting in higher V_{oc} for the former. This could be explained with the following facts. Compared with ZnO spheres, the ZnO ellipsoids have fewer grain boundaries, and the connectivity between nanoparticles building blocks is better, which results in fewer electron trapping/detrapping events at particle–particle interfaces; thereby, a reduced charge recombination and longer electron lifetime can be expected.

Electron diffusion coefficient ($D_n=d^2/(4\times\tau_d)$; d is the film thickness) of the DSSCs is insensitive to light intensity (Fig. 7b). The D_n of **Cell ZnO NRs+ellipsoids** is higher than that of **Cell ZnO NRs+spheres**. This significant improvement of electron transport can be related to the close packing of grains arising from the crystal intergrowth within the ellipsoids, which results in the excellent interior contacts between the constituent nanoparticles than ZnO spheres.

The charge collection efficiency (η_{cc}) of DSSCs in Fig. 7c can be estimated according to the electron transport time (τ_d) and lifetime (τ_r) ($\eta_{cc}=1-\tau_d/\tau_r$).[28, 29] The photocurrent density is described as $J_{sc}=q\eta_{lh}\eta_{inj}\eta_{cc}I_0$, where q is the elementary charge, η_{lh} is the light harvesting efficiency of a cell, η_{inj} is the charge-injection efficiency, η_{cc} is the charge-collection efficiency, and I_0 is light flux).[28] Fig. 7c shows the η_{cc} of **Cell ZnO NRs+ellipsoids** (96.78 %) is higher than that of **Cell ZnO NRs+spheres** (92.18 %).

Furthermore, the effective diffusion length ($L_n=(D_n\times\tau_r)^{1/2}$) of photoanode film suggests if the injected electron can transport to external circuit, which influences the overall J_{sc} and PCE. The L_n of the **Cell ZnO NRs+ellipsoids** (41.80 μm) is longer than that of **Cell ZnO NRs+spheres** (24.80 μm) (Fig. 7d), implying that **Cell ZnO NRs+ellipsoids** enable much more efficient electron transport. In this case, the thicker film is beneficial to further enhance photovoltaic performance without lowering the charge collection efficiency.

As an example, the detailed IMPS and IMVS parameters (τ_d, τ_r, η_{cc}, D_n and L_n) of DSSCs based on different double layered ZnO photoanodes measured under light intensity of 150 W/m^2 are

summarized in Table S2. Based on the discussions above, as compared to **Cell ZnO NRs+ellipsoids**, the more amounts of dye uptakes and superior light scattering ability for **Cell ZnO NRs+spheres** are responsible for the enhancement of power conversion efficiency.

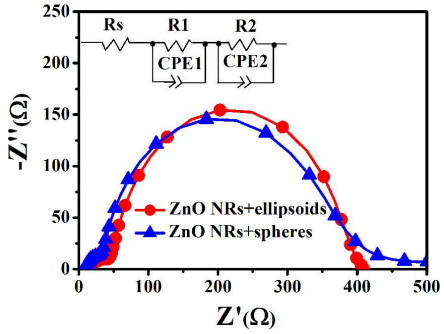

Fig. 8 Impedance spectra (Nyquist polts) of DSSCs based on different photoanodes (**ZnO NRs+ellipsoids**; **ZnO NRs+spheres**) measured in the dark at -0.6 V bias. And the inset illustrates the equivalent circuit simulated to fit the impedance spectrum.

The electrochemical impedance spectroscopy (EIS) as a steady state method is also utilized to study the kinetics of electrochemical and photoelectrochemical processes of DSSCs. Fig. 8 shows the Nyquist plots of the EIS results for the different ZnO films based DSSCs. The obtained plots contain two typical semicircles, which provide additional information and intensive understanding on the interfacial reactions of photoexcited electrons in DSSCs. The first small semicircle in the frequency range from 1 kHz to 1 MHz corresponds to a charge-transfer resistance in the redox electrolyte/Pt counter electrode interface. The similar value of the two DSSCs is due to the utilization of the same electrolyte and counter electrode in this work. The second large semicircle in the lower frequency range (0.1–1 kHz) is ascribed to the recombination resistance across the photoanode/dye/redox electrolyte interface. The charge recombination resistance (R_2, obtained from Z-view software) in **Cell ZnO NRs+ellipsoids** and **Cell ZnO NRs+spheres** are 36.80 Ω and 25.92 Ω, respectively. The larger R_2 for the former indicates the reduced recombination probability, which efficiently suppresses the back reaction of photo-generated electrons with I_3^- in the electrolyte within **Cell ZnO NRs+ellipsoids**. The **Cell ZnO NRs** (Supporting Information, Fig. S4) shows the largest R_2 (49.20 Ω) mainly due to the film (10 μm) is thinner than the double-layered films (15 μm), hence charge-recombination sites is less, which is in good concurrence with the aforementioned V_{oc} outcomes.

3. Experimental

3.1 Synthesis of ZnO ellipsoids and spheres

In a typical synthesis of ZnO spheres, 2.195 g of $Zn(CH_3COO)_2{\cdot}2H_2O$ is dissolved in the 60 mL diethylene glycol (DEG) in a 150 mL beaker, and 40 mL deionized water was added to the obtained solution, then 10 mL diethanolamine was added and further stirred for 30 min. Subsequently, the suspension are subjected to an intense ultrasonic irradiation (Sonics: VCX-500) for 10 min. The resultant precipitates are collected by centrifuging at 5000 rpm for 5 min, and washed with absolute ethanol and distilled water for five times, respectively. The resultant powders are dried at 60 °C for further characterizations. For comparison, the synthesis of ZnO ellipsoids is also performed in the absence of DEG with similar experimental conditons and processes.

3.2 Synthesis of ZnO nanorods (NRs)

The ZnO seed layer/FTO glass [30] is transferred to a 100 mL Teflon-lined stainless steel autoclave containing 0.892g $Zn(NO_3)_2{\cdot}6H_2O$, 0.048 g polyethylenimine and 0.420g hexamethylenetetramine (HMT) aqueous solution, then 4 mL $NH_3{\cdot}H_2O$ is added and further stirred for 30 min. And the hydrothermal reaction occurred at 88 °C for 7 h to obtain ZnO nanorod (NRs) arrays on FTO glass.

3.3 Fabrication of ZnO paste

1.0 g hierarchical ZnO ellipsoids or ZnO spheres samples are ground for 40 min in the mixtures of 8.0 mL ethanol, 0.2 mL acetic acid, 3.0 g terpineol and 0.5 g ethyl cellulose to form slurry. Then the mixtures are sonicated for 5 min in an ultrasonic bath, finally to form viscous ZnO ellipsoids or ZnO spheres paste.

3.4 Preparation of the working photoanode

ZnO ellipsoids or ZnO spheres layer （~5.0 μm） is screen-printed onto FTO/ZnO NRs substrate (~10.0 μm). The as-prepared double-layered films (ZnO NRs+ ZnO ellipsoids or ZnO NRs+ZnO spheres) are gradually heated under an air flow at 325 °C for 5 min, 375 °C for 5 min, 450 °C for 15 min, and 500 °C for 15 min, respectively. The as-fabricated photoanodes are immersed into N719 dye ($Ru[LL'\text{-}(NCS)_2]$, L=2,2'-bipyridyl-4,4'-dicarboxylic acid, L=2, 2'-bipyridyl-4, 4'-ditetrabutylammonium carboxylate, 5.0×10^{-4} M, Solaronix Co.) in acetonitrile/tert-butanol (volume ratio 1 : 1) solution, and were kept for 2 h at room temperature. Typically, we defined the DSSCs based on different anode materials films as follows: **ZnO NRs**: ~ 10 μm ZnO NRs; **ZnO NRs+ellipsoids**: ~ 10 μm ZnO NRs + ~ 5.0 μm ZnO ellipsoids; **ZnO NRs+spheres**: ~ 10 μm ZnO NRs + ~ 5.0 μm ZnO spheres.

3.5 Fabrication of DSSCs

The Pt-coated FTO glass counter electrode is prepared by dropping H_2PtCl_6 (5.0×10^{-4} M) solution onto the FTO glass followed by heating at 400 °C for 15 min in air. The electrolyte consists of 1-propyl-3-methyl-imidazolium iodide (PMII, 0.6 M), I_2 (0.03 M), LiI (0.05M), Guanidine thiocyanate (GuNCS) (GSCN, 0.1 M, Aldrich), and 4-tert-butylpyridine (t-BP, 0.5 M, Aldrich) in acetonitrile and valeronitrile (85:15 v/v). The active area of the N719-sensitized ZnO films is approximately 0.16 cm^2.

3.6 Characterization

The phase purity of the products is characterized by powder X-ray diffraction (XRD) on a Bruker D8 Advance X-ray diffractometer using Cu K_α radiation (λ=1.5418 Å), with an operating voltage of 40 kV and a current of 40 mA. The Field emission scanning electron

microscopy (FE-SEM, SU8010) are carried out to measure the morphology of as-prepared samples. Transmission electron microscope (TEM) and high-resolution transmission electron microscope (HR-TEM) and selected area electron diffraction (SAED) patterns are performed on a JEOL-2010 HR transmission electron microscope to futher determined the intrinsic structure. UV-vis diffuse reflectance spectra are measured on a UV-Vis-NIR Spectrophotometer (UV, Shimadzu UV-3600). The N_2 adsorption-desorption isotherms the hierarchical ZnO ellipsoids and spheres were measured by using an ASAP 2010 Surface Area Analyzer (Micromeritics Instrument Corporation).The thicknesses of ZnO films are measured by using a profilometer (Surface Profilomer, XP-2). The current–voltage characteristics are performed using a Keithley 2400 source meter under simulated AM 1.5 G illumination (100 mW cm^{-2}) provided by solar simulator (69920, 1 kW Xe lamp, Oriel). The incident light intensity is calibrated with a NREL-calibrated Si solar cell. Incident photon-to-current conversion efficiency (IPCE) signal is recorded on a Keithley 2000 multimeter under the illumination of a 150 W tungsten lamp with a Spectral Product DK240 monochrometer. Intensity-modulated photovoltage spectroscopy (IMVS) and intensity-modulated photocurrent spectroscopy (IMPS) are characterized on the electrochemical workstation (Zahner, Zennium) with a frequency response analyzer under a modulated blue light emitting diodes (457 nm) driven by a Zahner (PP211) source supply. The electrochemical impedance spectroscopy (EIS) measurements are performed with a Zennium electrochemical workstation (ZAHNER) at bias potential of -0.60 V in dark with the frequency ranging from 10 mHz to 1MHz.

4. Conclusions

In summary, the ZnO ellipsoids and spheres are successfully synthesized via a facile sonochemical process. The prepared ZnO ellipsoids and spheres have been demonstrated as excellent light scattering layers in DSSCs. The DSSCs based on 1D/3D double layered **ZnO NRs+ellipsoids** and **ZnO NRs+spheres** photoanodes shows a superior photovoltaic performance as compared to that of cells based on single layered **ZnO NRs**. The enhanced cell performance can be mainly ascribed to the more dye loading and superior light scattering ability resulting from introduce of ZnO ellipsoids and spheres as scattering layer. The present work can be extended to a wide arrange of applications, such as quantum dot sensitized solar cells, solid-state solar cells, perovskite solar cells, etc.

Acknowledgements

The authors acknowledge the financial supports from the Key Project of Tianjin Municipal Natural Science Foundation of China (13JCZDJ33900 and 14JCZDJC32200), National Natural Science Foundation of China (51502205, 51272176), Open Project of Key Laboratory of Advanced Energy Materials Chemistry (Nankai University) , Ministry of Education, Open Project of Key Laboratory of Functional Inorganic Material Chemistry (Heilongjiang University), Ministry of Education, the Scientific Research Foundation of Tianjin Normal University (5RL131), and Academic Innovation Funding of Tianjin Normal University (52XC1404).

Notes and references

1 B. O'Regan and M. Grätzel, *Nature* 1991, **353**, 737.
2 M. Grätzel, *Nature* 2001, **414**, 338.
3 S. Mathew, A. Yella, P. Gao, R. Humphry-Baker, B. F. E. Curchod, N. Ashari-Astani, I. Tavernelli, U. Rothlisberger, M. K. Nazeeruddin and M. Grätzel, *Nature Chemistry*., 2014, **6**, 242.
4 C. X. He, B. X. Lei, Y. F. Wang, C. Y. Su, Y. P. Fang and D.B. Kuang, *Chem. -Eur. J.,* 2010, **16**, 8757.
5 Z. Dong, X. Lai, J. E. Halpert, N. Yang, L.Yi, J. Zhai, D. Wang, Z. Tang and L. Jiang, *Adv. Mater*., 2012, **24**,1046.
6 Y. F. Wang, K. N. Li, C. L. Liang, Y. F. Hou, C. Y. Su and D. B. Kuang, *J. Mater. Chem*., 2012, **22**, 21495.
7 Y. F. Wang, J. W. Li. Y. F. Hou, X. Y. Yu, C. Y. Su and D. B. Kuang, *Chem. -Eur. J.,* 2010, **16**, 8620.
8 G. Shang, J. Wu, S. Tang, M. Huang, Z. Lan, Y. Li, J. Zhao and X. Zhang, *J. Mater. Chem*., 2012, **22**, 25335.
9 Y. F. Wang, K. N. Li, Y. F. Xu, H. S. Rao, C. Y. Su and D. B. Kuang, *Nanoscale*., 2013, **5**, 5940.
10 Z. Li, Y. Zhou, C. Bao, G. Xue, J. Zhang, J. Liu, T. Yu and Z. Zou, *Nanoscale*., 2012, **4**, 3490.
11 Y. F. Li, Y. Wang, C. Y. Chen, A. Y. Pang and M. D. Wei, *Chem. -Eur. J*., 2012, **18**, 11716.
12 Y. F. Li, X. Z. Zheng, H. X. Zhang, B. B. Guo, A. Y. Pang and M. D. Wei, *Electrochim. Acta*., 2011, **56**, 9257.
13 E. M. Kaidashev, M. Lorenz, H. Wenckstern, A. von; Rahm, H. C. Semmelhack, K. H. Han, G. Benndorf, C. Bundesmann,H. Hochmuth and M. Grundmann, *Appl. Phys. Lett*., 2003, **82**, 3901.
14 L. E. Greene, B. D. Yuhas, M. Law, D. Zitoun and P. D. Yang, *Inorg. Chem*., 2006, **45**, 7535.
15 M. Law, L. Greene, J. C. Johnson, R. Saykally and P. Yang, *Nat. Mater*., 2005, 4, 455.
16 M. Guo, P. Diao, X. D. Wang and S. M. Cai, *J. Solid State Chem*., 2005,**178**, 3210.
17 J. J. Kim, K. S. Kim and G. Y. Jung, *J. Mater. Chem*., 2011, **21**, 7730.
18 D. B. Kuang, J. Brillet, P. Cher, M. Takata, S. Uchida, H. Miura, K. Sumioka, S. M. Zakeeruddin and M. Grätzel, *ACS Nano*., 2008, **2**, 1113.
19 W. Q. Wu, H. S. Rao, H. L. Feng, X. D. Guo, C. Y. Su and D. B. Kuang, *J. Power Sources*., 2014, **260**, 6.
20 D. H. Chen, F. Z. Huang, Y. B. Cheng and R. A. Caruso, *Adv. Mater*., 2009, **21**, 2206.
21 M. Ye, D. Zheng, M. Lv, C. Chen, C. Lin and Z. Lin, *Adv. Mater*., 2013, **25**, 3039.
22 Y. J. Xiong, H. G. Cai, B. J. Wiley, J. G. Wang, M. J. Kim and Y. N. Xia, *J. Am. Chem. Soc.,* 2007, **129**, 3665.
23 F. De Angelis, S. Fantacci, E. Mosconi, M. K. Nazeeruddin and M. Grätzel, *J. Phys. Chem. C* 2011, **115**, 8825.
24 G. Schlichthorl, S.Y. Huang, J. Sprague and A. J. Frank, *J. Phys. Chem. B* 1997, **101**, 8141.
25 B. C. O'Regan, K. Walley, M. Juozapavicius, A. Anderson, F. Matar, T. Ghaddar, S. M. Zakeeruddin, C. Klein and J. R. Durrant, *J. Am. Chem. Soc.,* 2009, **131**, 3541.
26 H. X. Wang, P. G. Nicholson, L. Peter, S. M. Zakeeruddin and M. Grätzel, *J. Phys. Chem. C* 2010, **114**, 14300.
27 T. Oekermann, T. Yoshida, H. Minoura, K. G. U. Wijayantha and L. M. Peter, *J. Phys. Chem. B* 2004, **108**, 8364.
28 K. Zhu, N. R. Neale, A. Miedaner and A. J. Frank, *Nano Lett*., 2007, **7**, 69.
29 T. Oekermann, D. Zhang, T. Yoshida and H. Minoura, *J. Phys. Chem. B* 2004, **108**, 2227.

30 Q. P. Luo, B. X. Lei, X. Y. Yu, D. B. Kuang and C. Y. Su, *J. Mater. Chem.*, 2011, **21**, 8709.

TOC

The ZnO ellipsoids and spheres are fabricated via a facile sonochemical process. Dye-sensitized solar cells based on 1D/3D double layered ZnO photoanode are designed. The ZnO ellipsoids and spheres show superior light scattering ability in DSSCs.